ARMY RESEARCH LABORATORY

Electro-Thermal Igniter (ETI) Particle Deposition Upon a Simulated Propellant Surface

by Stephen L. Howard

ARL-TR-4377 February 2008

NOTICES

Disclaimers

Army Research Laboratory
Aberdeen Proving Ground, MD 21005-5066

ARL-TR-4377 **February 2008**

Electro-Thermal Igniter (ETI) Particle Deposition Upon a Simulated Propellant Surface

Stephen L. Howard
Weapons and Materials Research Directorate, ARL

REPORT DOCUMENTATION PAGE	*Form Approved* *OMB No. 0704-0188*

Public reporting burden for this collection of information is estimated to average 1 hour per response, including the time for reviewing instructions, searching existing data sources, gathering and maintaining the data needed, and completing and reviewing the collection information. Send comments regarding this burden estimate or any other aspect of this collection of information, including suggestions for reducing the burden, to Department of Defense, Washington Headquarters Services, Directorate for Information Operations and Reports (0704-0188), 1215 Jefferson Davis Highway, Suite 1204, Arlington, VA 22202-4302. Respondents should be aware that notwithstanding any other provision of law, no person shall be subject to any penalty for failing to comply with a collection of information if it does not display a currently valid OMB control number.
PLEASE DO NOT RETURN YOUR FORM TO THE ABOVE ADDRESS.

1. REPORT DATE ***(DD-MM-YYYY)***	**2. REPORT TYPE**	**3. DATES COVERED (From - To)**
February 2008	Final	October 2005 through December 2007

4. TITLE AND SUBTITLE Electro-Thermal Igniter (ETI) Particle Deposition Upon a Simulated Propellant Surface	**5a. CONTRACT NUMBER**
	5b. GRANT NUMBER
	5c. PROGRAM ELEMENT NUMBER
6. AUTHOR(S) Stephen L. Howard (ARL)	**5d. PROJECT NUMBER** 622618.H8000
	5e. TASK NUMBER
	5f. WORK UNIT NUMBER
7. PERFORMING ORGANIZATION NAME(S) AND ADDRESS(ES) U.S. Army Research Laboratory Weapons and Materials Research Directorate Aberdeen Proving Ground, MD 21005-5066	**8. PERFORMING ORGANIZATION REPORT NUMBER** ARL-TR-4377
9. SPONSORING/MONITORING AGENCY NAME(S) AND ADDRESS(ES)	**10. SPONSOR/MONITOR'S ACRONYM(S)**
	11. SPONSOR/MONITOR'S REPORT NUMBER(S)

12. DISTRIBUTION/AVAILABILITY STATEMENT

Approved for public release; distribution is unlimited.

13. SUPPLEMENTARY NOTES

14. ABSTRACT

An experimental investigation was performed to gain insights into the flows resulting from a plasma jet impinging on a flat plate at representative incident angles of 90, 60, and 45 degrees in the open air for two plasma pulse lengths (~0.3 and 1.0 ms) and two plasma energies (0.7 and 1.3 kJ). Specifically, the investigation characterized the influence of the pulse length, pulse energy, and angle on particle deposition on a flat simulated propellant surface in an attempt to clarify the effect of plasma-propellant interactions occurring during the electro-thermal ignition of a propellant charge system. Comparisons of data from the flow signature on impingement plates showed that although a plasma jet with a short pulse length may be more powerful, the shorter time duration of flow reduced the number of particles that were deposited. Therefore, the pulse length may be a key parameter needed to be optimized in order to effectively ignite a propellant charge system with a minimum demand of electrical energy. Differences in deposition at variable incident angles of jet impingement were also evident.

15. SUBJECT TERMS

ETC, ETI, plasma ignition, high loading-density propellant charges, impingement flow

16. SECURITY CLASSIFICATION OF:			**17. LIMITATION OF ABSTRACT**	**18. NUMBER OF PAGES**	**19a. NAME OF RESPONSIBLE PERSON** Stephen L. Howard
a. REPORT Unclassified	**b. ABSTRACT** Unclassified	**c. THIS PAGE** Unclassified	SAR	25	**19b. TELEPHONE NUMBER** (*Include area code*) 410-278-6098

Standard Form 298 (Rev. 8/98)
Prescribed by ANSI Std. Z39.18

Contents

List of Figures

Acknowledgments

The author would like to express his appreciation to Dr. Lang-Mann Chang of American Systems Corporation, 13990 Parkeast Circle, Chantilly, VA 20151, currently stationed at the U.S. Army Research Laboratory (ARL), Aberdeen Proving Ground (APG), Maryland, for his assistance in initiating this type of investigation. The author would also like to thank Dr. Michael A. Schroeder currently stationed at ARL, APG, in the position of Emeritus for his help in obtaining x-ray fluorescence spectra of the plasma deposits.

INTENTIONALLY LEFT BLANK

1. Introduction

Substantial research activities have been conducted on the subject of plasma-propellant interactions, and significant progress has been made toward understanding various aspects of the interactions. Among the efforts, measurements have been made, to some extent, for pressure (*1*), temperature, and plasma density distributions at specific axial distances from the plasma source. Significant work has also been performed on characterization of the plasma flow inside a closed chamber, flow patterns in a gun chamber packed with inert propellant discs, and chemical analyses of plasma-exposed propellant samples (*2*, *3*). Continuing research efforts are certainly needed to provide a better understanding of the flow interaction in advancing this novel propulsion technology.

Some new studies have indicated that metal particles, whether from the fuse wire that initiates the plasma or from the eroding capillary nozzle, could be a major contributor to the ignition process (*4*). One goal of the present study is to determine to what extent these metal particles would be deposited in or on a simulated propellant surface.

2. Experimental

The present study experimentally characterized a plasma jet flow in open air that impinged on a flat plate positioned at various angles at a distance of approximately 2.5 cm from the incoming jet stream. The plasma pulse length was also varied from 0.3 to nearly 1 ms. The plasma was generated within a polyethylene tube (~3.2 mm inside diameter) with a thin nickel wire fuse (~0.13 mm diameter) connected to two electrodes in a stainless steel housing. The anode was fabricated from tungsten and the cathode from 4340 gun steel. The length-to-diameter ratio of the capillary tube was 12. Although the pulse power unit was capable of storing as much as 3 kJ, energies of 0.7 and 1.3 kJ were used in this study. High-speed video with a Phantom[1] V camera was obtained in order to record the flow phenomena, and witness sheets were installed over the impingement plate for a permanent record of particle deposition. Neutral density filters were used with the camera in order to reduce the overall luminosity to the point that the shock structures were visible. The impingement fixture (figures 1 and 2) had been developed earlier to obtain the pressure distribution on an impingement plate from an effusive plasma jet (*1*, *5*), and its usefulness was extended to this study.

The particles deposited on the witness sheets were examined with an x-ray fluorescence (XRF) instrument for elemental composition. The witness sheet surface conditions and particle morphology were examined with an International Scientific Instruments, Inc. SS40 scanning electron microscope (SEM).

[1]Phantom is a registered trademark of ViSiON Research, Inc.

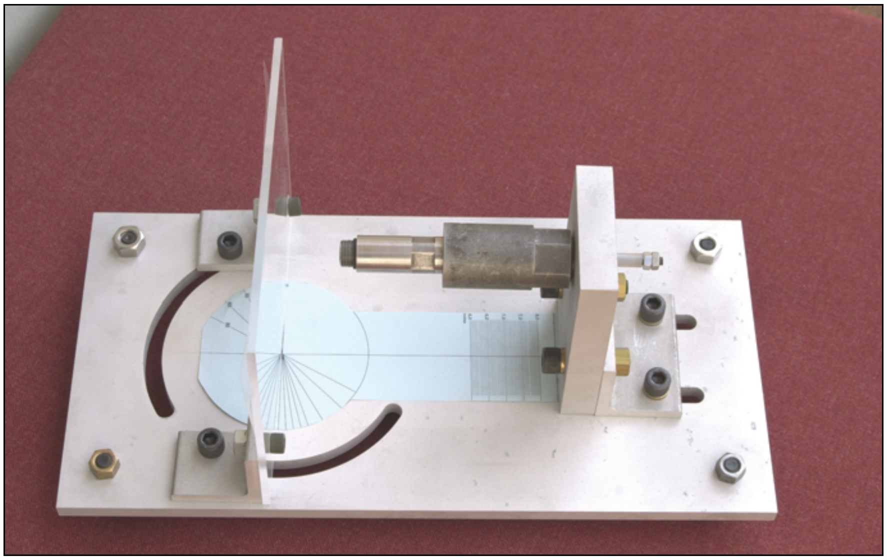

Figure 1. Photograph of side view of effusive plasma jet impingement plate fixture.

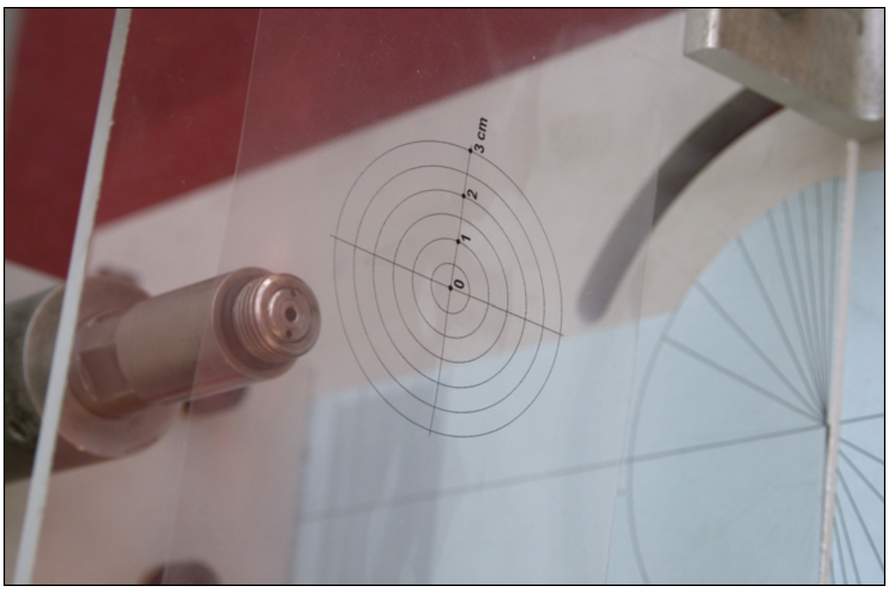

Figure 2. Photograph of effusive plasma jet impingement plate fixture showing witness plate (with inscribed circles); view from behind impingement plate.

3. Results and Discussion

A flat plate was the geometry chosen for this study since some propellant loading schemes have this geometry explicitly or could be modeled with the flat plate as a limit. The impingement data were collected as high-speed video of the plasma jet or as forensic evidence on a witness plate after the jet had ceased. The angles of incidence (90, 60, and 45 degrees) were also chosen as those that were easily available to the experiment and likely to be representative of the range of angles accessed by an effusive plasma jet upon a propellant surface close to the exhaust nozzle of the jet. Photographic evidence revealed, in general, a complex shock flow structure typically consisting of a barrel shock, a Mach disc, and a precursor shock.

However, the flow characteristics at constant energy (1.3 kJ in figure 3) varied profoundly with plasma pulse length. As shown in figure 3, the longer pulse length (approximately 1 ms in duration) resulted in an initially narrower flow field but much greater flow penetration depth in the open air than did the flow from the short pulse (approximately 0.3 ms in duration). This figure depicts the length of penetration of the jet into open air at 56% of each respective pulse duration (0.17 ms for the short pulse and 0.56 ms for the long pulse). Past this percentage of pulse length, the jet front of the long pulse exceeded the field of view (FOV) of the camera while the short pulse essentially dissipated to a non-visible cloud within the same FOV. The longer pulse also produced a peak luminosity that was less than the short pulse, but as might be expected, the luminous part of the flow lasted a longer time. Additionally, the flow signatures on the impingement plate (figure 4) displayed over a diameter of 18 cm were significantly different for the two pulse lengths. These variations should have a strong effect on plasma-propellant interaction and thus on the effectiveness of propellant ignition.

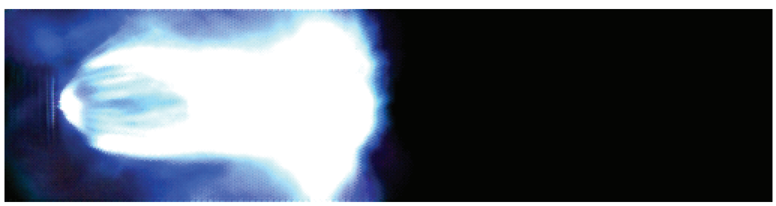
(a)

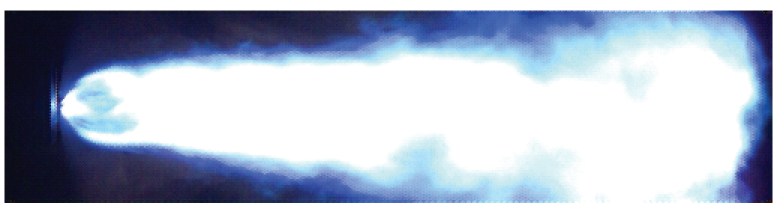
(b)

Figure 3. Comparison of distance traveled by the jet front at 56% of respective pulse duration (a) short pulse, and (b) long pulse at 1.3 kJ.

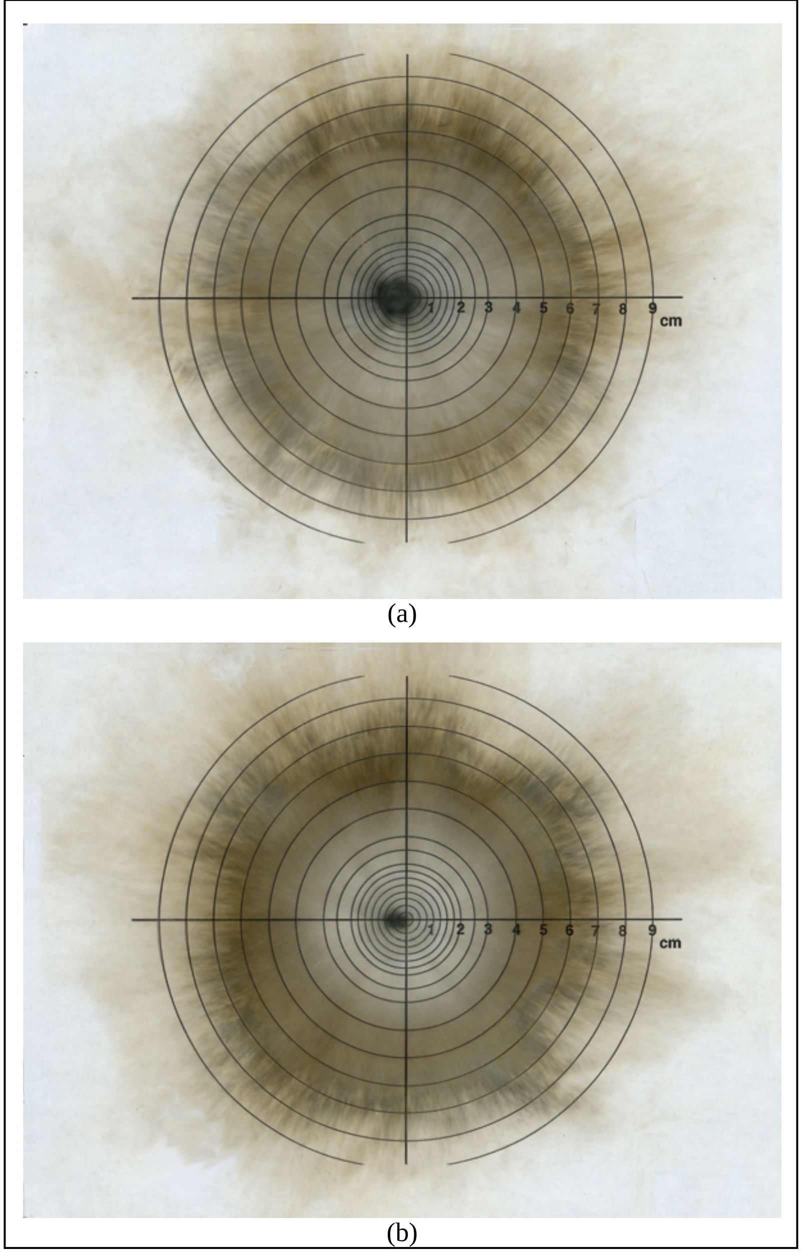

Figure 4. Comparison of impingement signature of a (a) short pulse, and (b) long pulse at an incidence angle of 90 degrees at 1.3 kJ.

As the incident angle of the impingement plate was decreased from 90 degrees, the shape of the jet interaction with the plate changed. Particle deposition measurements also were taken at 60 and at 45 degrees for a total of three incident angles. The high-speed visualizations of the angular extremes are presented in figures 5 through 8 (at 90 and at 45 degrees). The visualization of the jet during the period of high-pressure flow at an angle normal to the impingement surface is presented in figures 5 and 6. Figure 5 shows the jet at a short pulse length, and figure 6 shows the jet at a long pulse length. Figures 7 and 8 visualize the same pulse lengths, respectively, of the jet flow at an impingement angle of 45 degrees during the impinging event.

Figure 5. Frames of high-speed video showing visualization of a short pulse impinging on a plate at an incident angle of 90 degrees (20,000 frames per second).

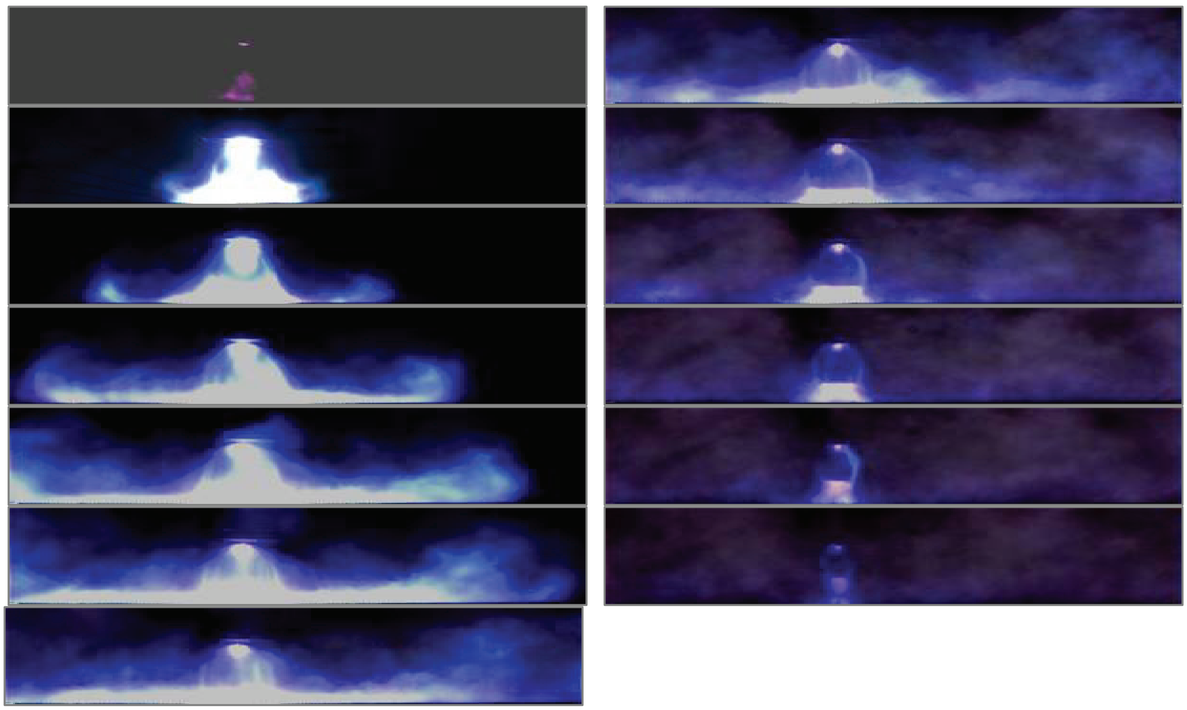

Figure 6. Frames of high-speed video showing visualization of a long pulse impinging on a plate at an incident angle of 90 degrees at 1.3 kJ (13,100 frames per second).

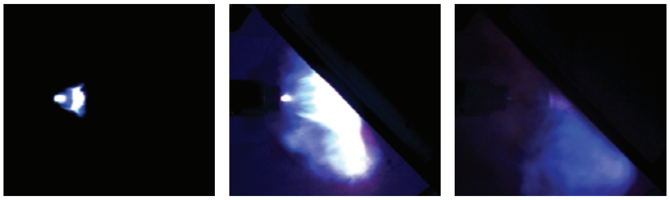

Figure 7. Frames of high-speed video showing visualization of a short pulse impinging on a plate at an incident angle of 45 degrees at 1.3 kJ.

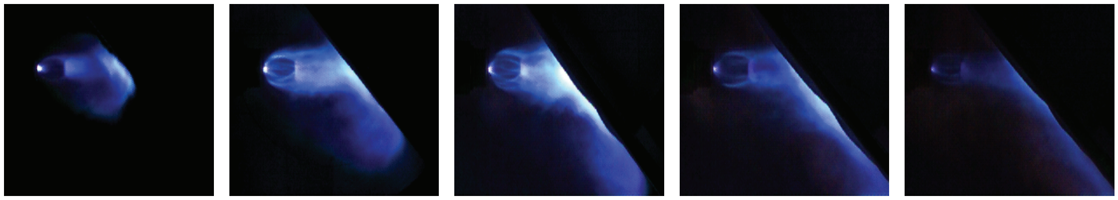

Figure 8. Frames of high-speed video showing visualization of a long pulse impinging on a plate at an incident angle of 45 degrees at 1.3 kJ.

If the visual emission from the effusing gases is assumed to provide a qualitative measure of local temperature, the propellant surface upon which the jet impinged could be expected to react differently with the two pulse lengths (e.g., view figures 5 and 6). The short pulse appeared to have the highest temperature gases impinge upon a relatively small surface as compared to the long pulse. This region also experienced the largest pressure (as measured in an earlier study [*4*]) on the impingement plate. The hot gases from the short pulse then dissipated rapidly as compared to the long pulse. Although hot gas and high pressure are good initiation conditions for most propellants, the time duration of the conditions can also be a factor. If the short pulse develops too much pressure, propellant can be fractured locally and a possible undesirable high-rate burning region may be created with pressure waves later in the ballistic cycle (*6*, *7*). However, if the pulse is much too short for effective ignition, only the surface of the propellant would be affected, and heat loss or ablation of a very thin reacting layer away from the propellant surface may quench an otherwise promising ignition.

From the comparison of the visualizations in figures 7 and 8, the effective heated surface of the impacted propellant at an incident angle of 45 degrees would be even smaller than at normal incidence. Figure 7 shows some of the hot flow lifting off the surface and thus reducing its effectiveness. Whether other adjoining propellant grains would be able to use the energy in the misdirected flow, additional study would be needed. However, the total output energy of the jet would be impinging on additional surface area, and the energy density at any one point would be reduced, possibly to below the level for effective ignition. The long pulse behaved differently. The flow seemed to adhere to the surface and thus increase the time that the hot gases would be in contact with the propellant surface. The somewhat lower temperatures and pressures generated by the longer pulse could be compensated by the longer convective times in determining effective ignition levels.

Since hot particles can also influence/improve ignition (*8*), witness plates constructed of overhead slide material were placed on the impingement plate (figures 2, 4, and 9 through 13) and the spectral density of the resulting patterns obtained. Before examination of the witness plates with the SEM, it was assumed that since the plasma was generated in a polyethylene tube, the particles generated in the plasma jet would consist of primarily fine carbon particles with a small contribution from the fuse wire (nickel). It was also assumed that the nickel particle sizes would be quite small so that the nickel particles would have appeared to be black (in visible light) just like the carbon particles.

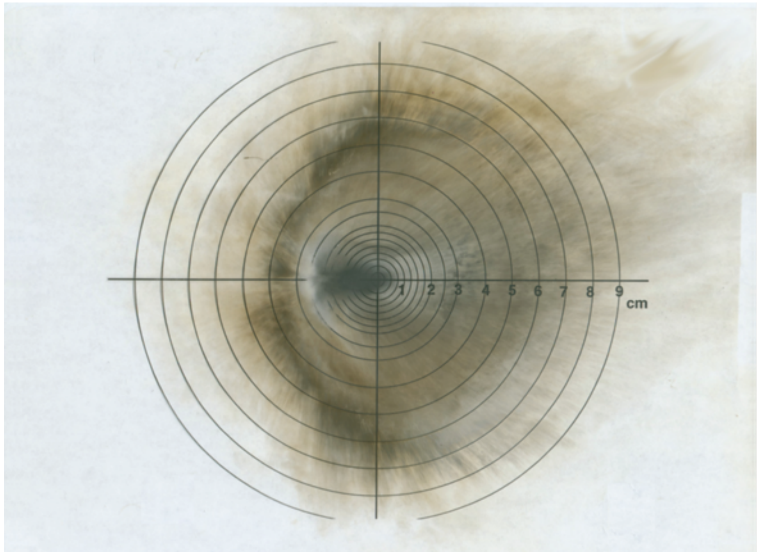

(a)

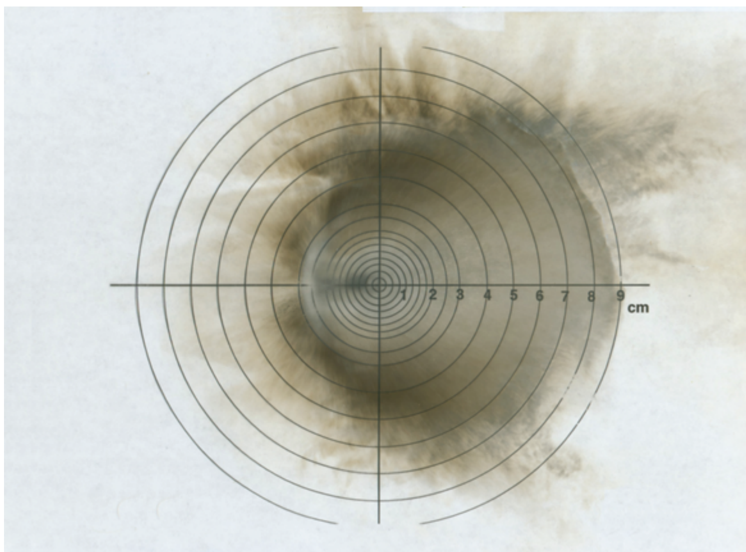

(b)

Figure 9. Comparison of impingement signature of a (a) short pulse and (b) long pulse at 1.3 kJ and 60-degree incidence angle.

As a test of this hypothesis, the witness plates[2] were examined by XRF. Since the material of the film was hydrocarbon in nature, spectra of carbon, hydrogen, and oxygen were ignored. The ink lines (placed on the film for spatial location information) “set down” by the laser printer contained iron so these regions were avoided for analysis.

Three regions on the witness plate were examined. First, a region near the edge of plate was examined as a base reference. Elements found were mainly carbon (C) and oxygen (O) on the

[2]A type of polyester film as a base substrate with electrostatic receptor layers comprised of thermoplastic resins such as polyester resins, styrene resins, polymethylmethacrylate resins, epoxy resins, or polyurethane resins

main surface of the plastic, with possible traces of copper (Cu), zinc (Zn), sodium (Na), silicon (Si), chlorine (Cl), and aluminum (Al). The lines inked on the surface of the plastic also showed some iron (Fe). The second region came from the brownish region relatively far from the center of the impingement, as seen in figure 10. The XRF spectrum of this sample showed the usual carbon and oxygen, as well as significant amounts of Fe, nickel (Ni), and small amounts of Al, chromium (Cr), and Si. The amounts of Fe and of Al appeared to be greater than could be accounted for by the base reference. The third region was sampled near the center of the impingement in the very dark area. The XRF spectrum of this sample showed significant amounts of Fe and Ni.

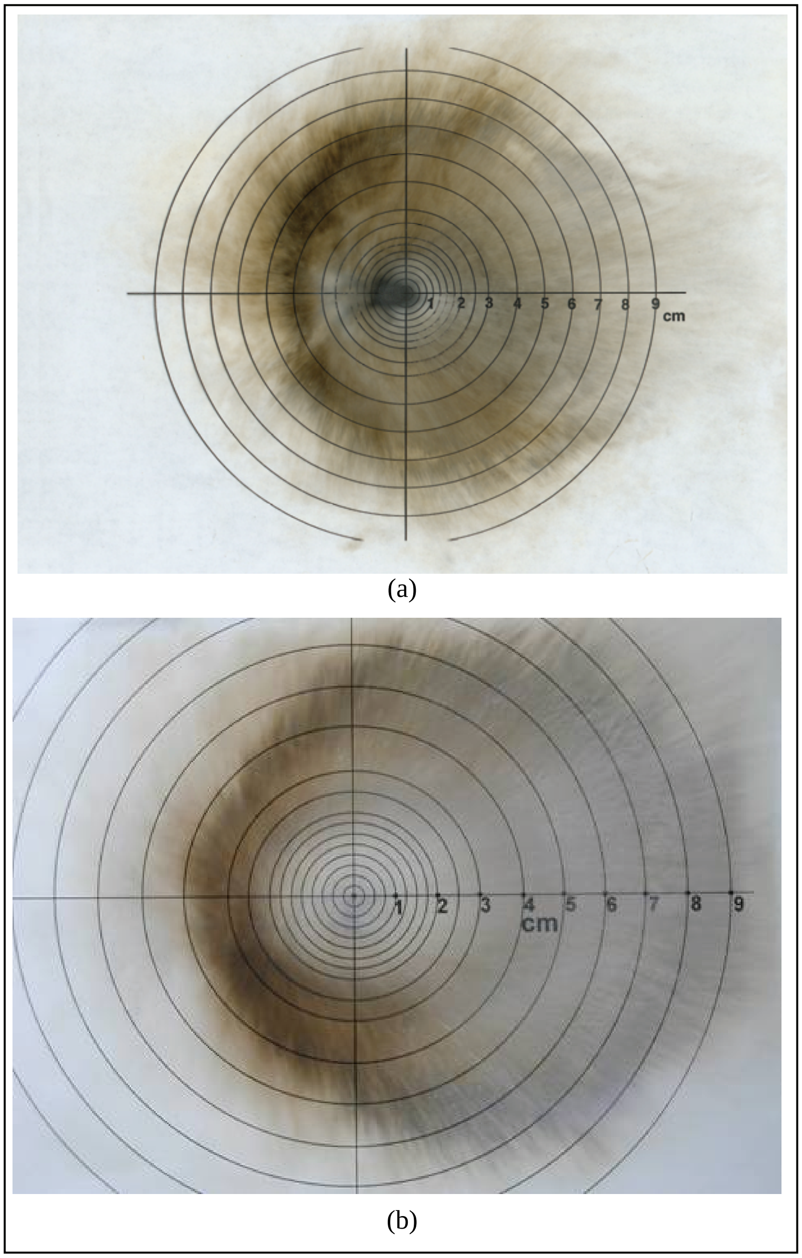

Figure 10. Comparison of impingement signature of a (a) short pulse and (b) long pulse at 1.3 kJ and 45-degree incidence angle.

Since Fe, Ni, Cr, and Si were found, the spectra were searched for manganese (Mn) and molybde-num (Mo). Mn and Mo were also found. These six elements are the primary constituents (the Ni from the fuse wire could not be distinguished from that possibly originating in the steel) of the steel alloy that formed the cathode nozzle of the plasma jet. Therefore, a substantial fraction of the particles carried by the plasma flow that were subsequently deposited were from the metals originating in the fuse wire and/or the cathode nozzle. It was unfortunate that XRF could not also discern the possible carbon agglomerates, or "soot," from the witness plate material since they should also have been formed abundantly.

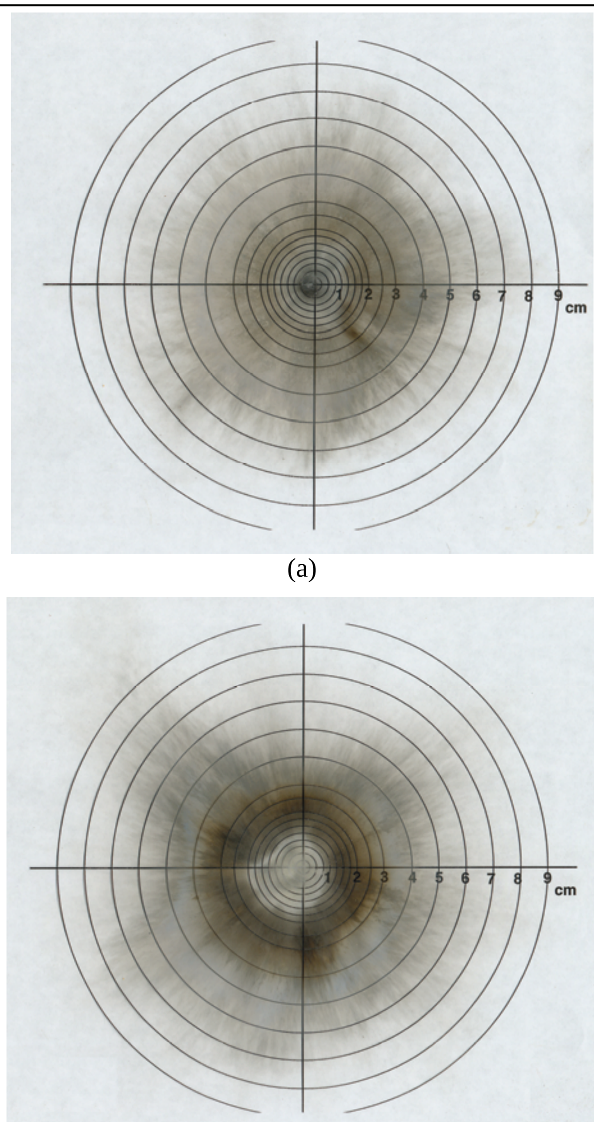

(a)

(b)

Figure 11. Comparison of impingement signature of a (a) short pulse and (b) long pulse at 0.7 kJ and 90-degree incidence angle.

Another useful "visual" diagnostic used to identify particles and the impingement surface itself was the SEM. In this technique, the surface of the witness plate and the particle morphology could be viewed rather easily at thousands of times magnification. Although the features discussed next were exhibited on all the witness plates shown in figures 4 and 9 through 13, only figure 4 (90-degree angle of incidence) is discussed. We mounted all the samples in the SEM views on an aluminum stub with a conductive carbon paint and then cold sputtered with gold/palladium using an SPI Supplies[3] sputter coater to provide a uniform conductive coating.

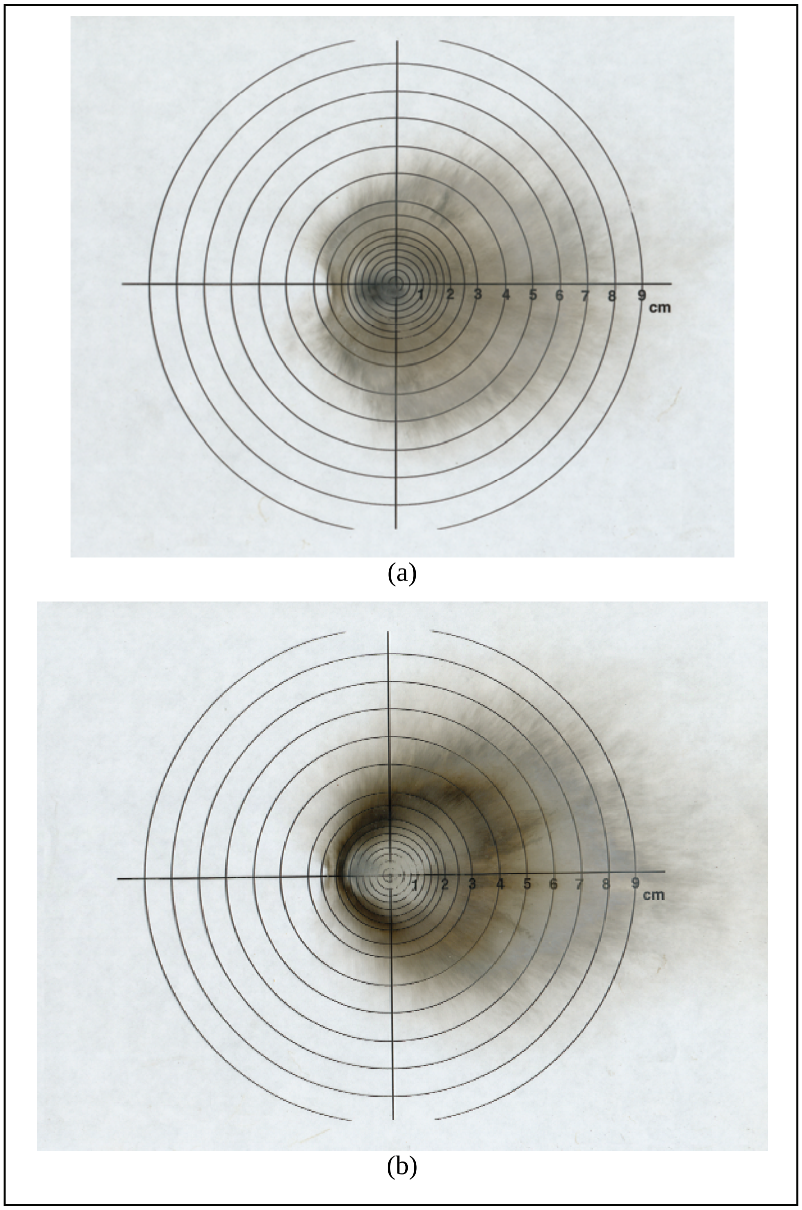

Figure 12. Comparison of impingement signature of a (a) short pulse and (b) long pulse at 0.7 kJ and 60-degree incidence angle.

[3]SPI Supplies is a registered trademark of Structure Probe, Inc.

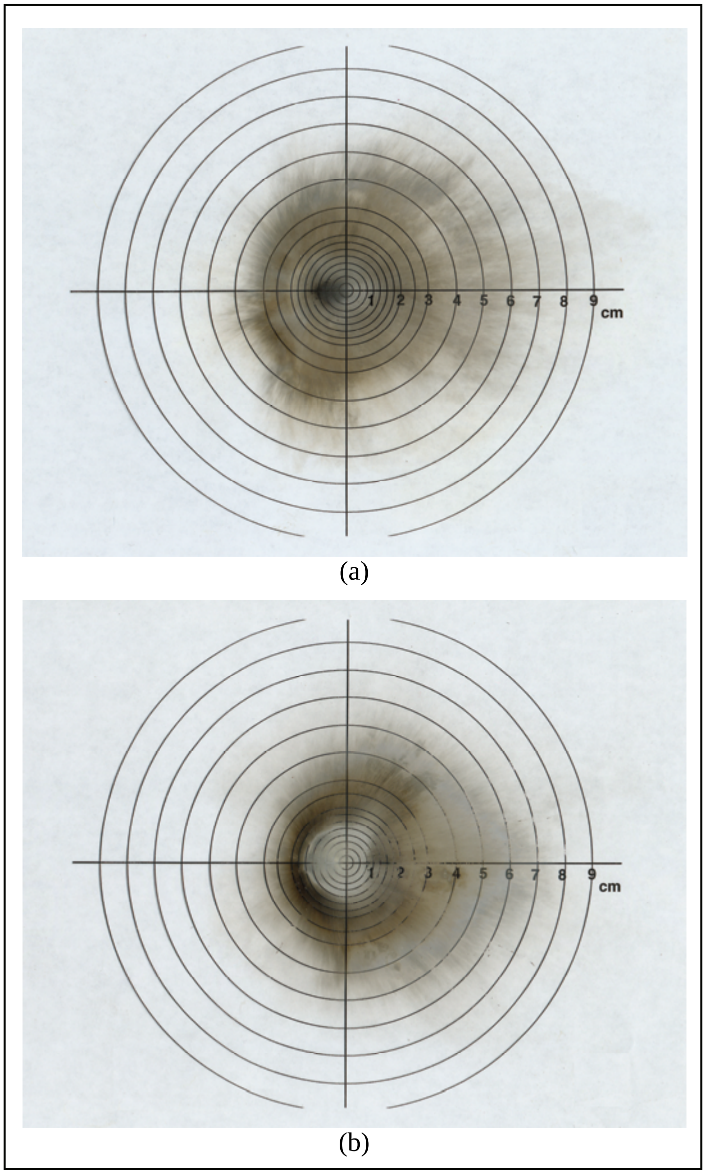

Figure 13. Comparison of impingement signature of a (a) short pulse and (b) long pulse at 0.7 kJ and 45-degree incidence angle.

A set of reference views of the witness plate material was obtained to provide an initial survey of the surface. These views are shown in figures 14 and 15. Other than a few relative large particles of dust shown in figure 14 at low magnification (magnification of 17), the surface is relatively smooth without imperfections (see figure 15 at a magnification of 10,000).

The witness plates shown in figure 4 (incidence angle of 90 degrees) were contrasted to the reference views in figures 14 and 15. The samples for the contrast were taken from two locations from each of the two witness plates in figure 4. One location (labeled "6-cm" location) was just to the left of vertical axis at the 6-cm radius line (sample taken from the brownish area), and the other location (labeled “center” location) was just to the left of the center of impingement (sample taken from the blackish region).

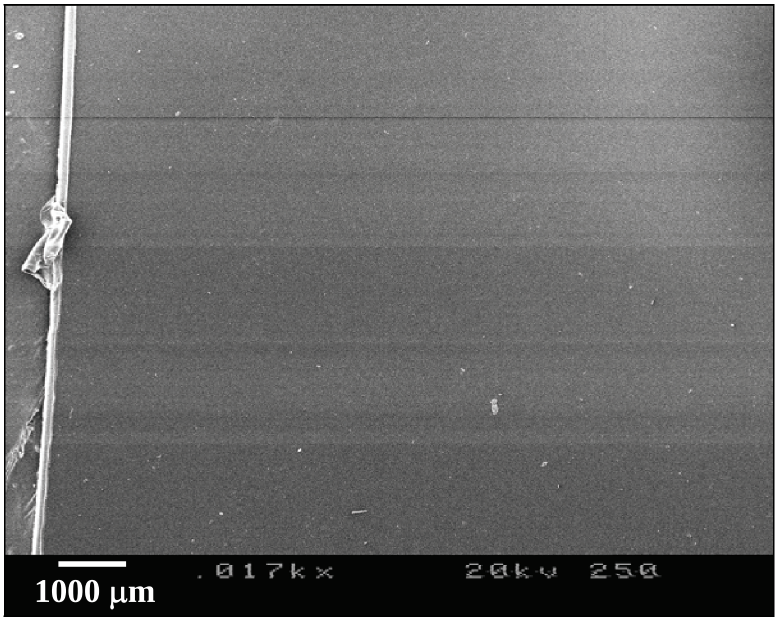

Figure 14. SEM view at magnification of 17 of virgin witness plate material.

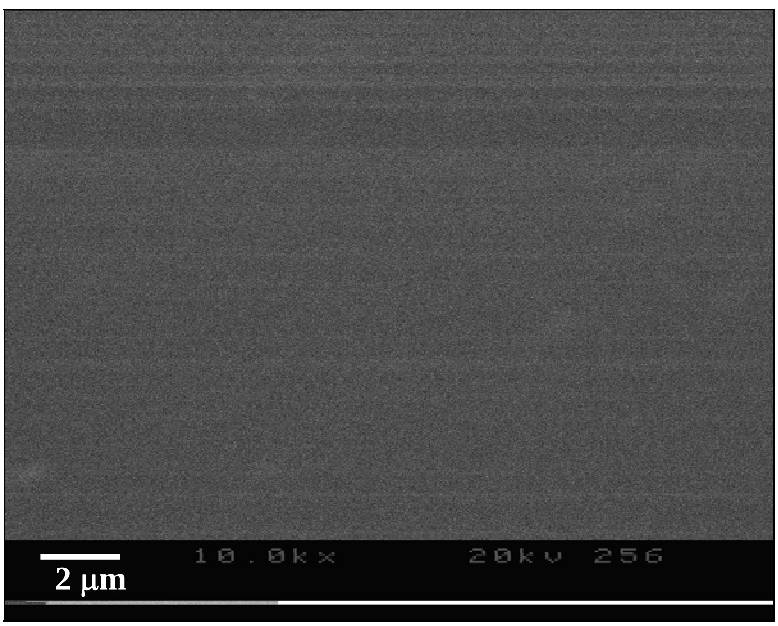

Figure 15. SEM view at magnification of 10,000 of virgin witness plate material showing lack of surface imperfections.

Figures 16 through 25 were formed by a plasma pulse length of 1 ms, and figures 26 through 36 were formed by a pulse length of 0.3 ms. Figures 16 through 20 and 26 and 27 show surface damage in the form of relatively large scrapes or gouges that most likely were present before exposure to the plasma jet. This damage was not noticeably evident to the naked eye before examination by the SEM. Figures 18 and 19 show damage to the surface, which can be traced to the plasma jet. Short gouge tracks on the order of a few microns wide and tens of microns long were present. All the gouge tracks were aligned in the same direction—away from what could be traced to the impingement center. All these tracks began as shallow and deepened until abruptly ending, usually with what appears to be a "splash" of the material removed from the gouge. It is unclear whether the particle that created the track is imbedded under the surface of the witness plate material, if it is contained within the splash material, or if it left the surface after exiting the track and was swept away.

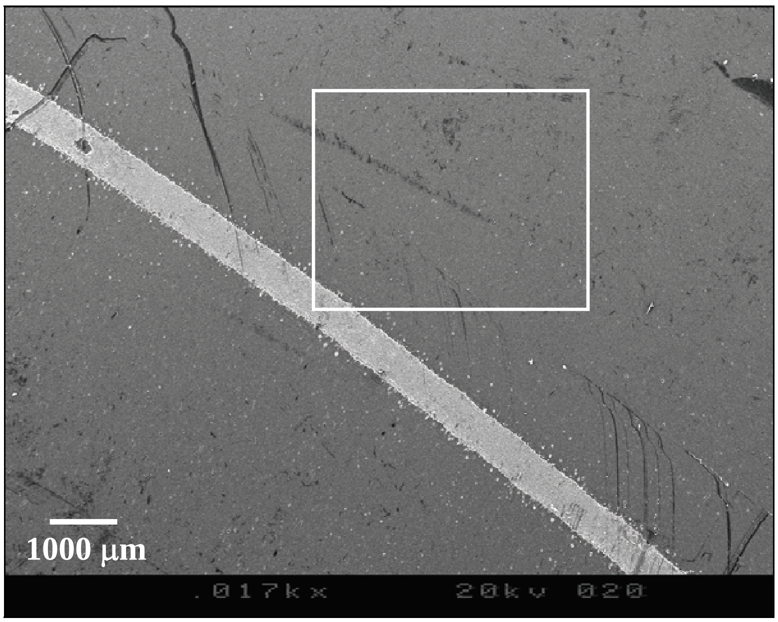

Figure 16. SEM view at magnification 17 of a 6-cm location (plasma pulse length of 1 ms) showing laser printer line (white strip through center) and white box showing approximate location of next higher magnification view.

Other particles seem to be simply deposited on the surface. Figures 17 through 20 show randomly shaped particles that range from a few microns to submicron in size. There does not seem to be any orientation to these particles. Therefore, it appears that there were at least two types of particles, one that had sufficient momentum and internal energy to deform the surface, and another that did not.

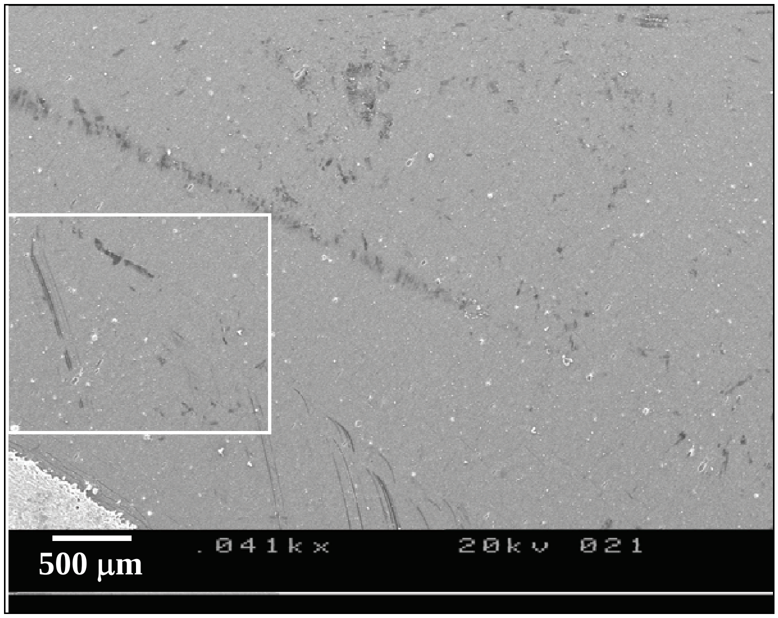

Figure 17. SEM view at magnification 41 of a 6-cm location (plasma pulse length of 1 ms) with white box showing approximate location of next higher magnification view.

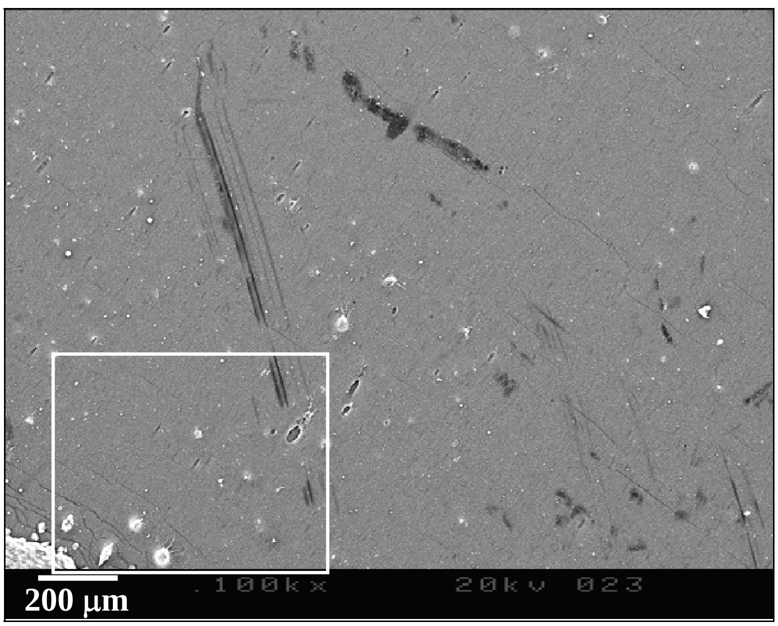

Figure 18. SEM view at magnification 100 of a 6-cm location (plasma pulse length of 1 ms) with white box showing approximate location of next higher magnification view.

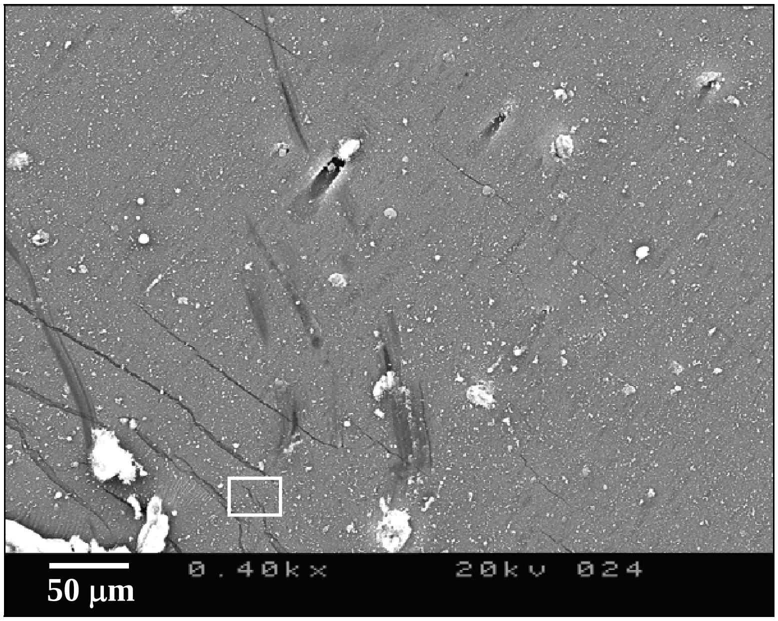

Figure 19. SEM view at magnification 400 of a 6-cm location (plasma pulse length of 1 ms) with white box showing approximate location of next higher magnification view.

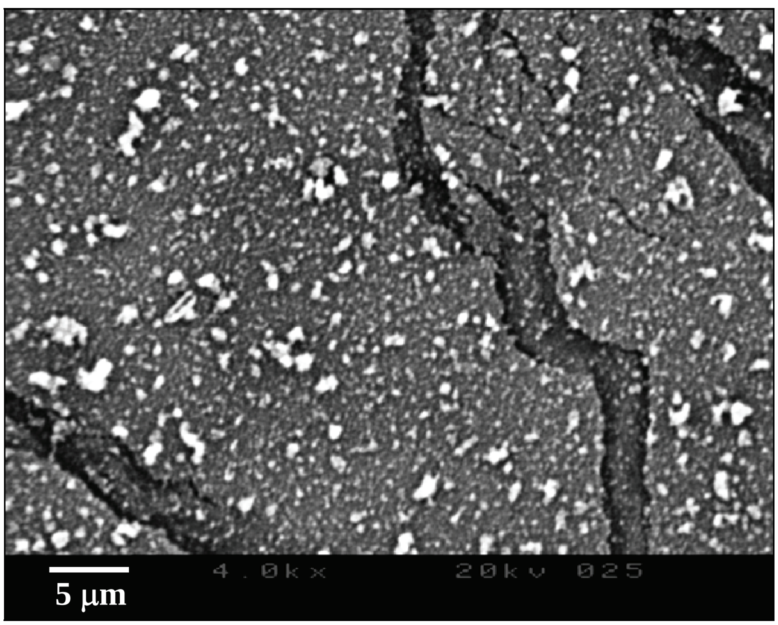

Figure 20. SEM view at magnification 4,000 of a 6-cm location (plasma pulse length of 1 ms).

The surface landscape near the impingement center was greatly different than at the rather large distance of 6-cm radius. Figures 21 through 25 show a surface that is pocked and distorted. The edges of the “craters” appear to be thermally distorted, and some of the craters appear to have been formed by a particle that became deeply imbedded in the witness plate material. Other distortions appear as “channels”. The channels resemble thermal distortion and/or partial melting of thin layer material on a substrate. It is most likely that the channels were formed by the impingement of hot gases on the thin electrostatic receptor layers on the polyester substrate that comprised the witness plate material. Further evidence of melting is found in figure 25 where myriads of fine particles appear to be mostly submerged in the surface material with a thin smooth layer of surface material above them. The particles were likely deposited during an early phase of jet flow, and then melting of the surface layers by hot gases occurred.

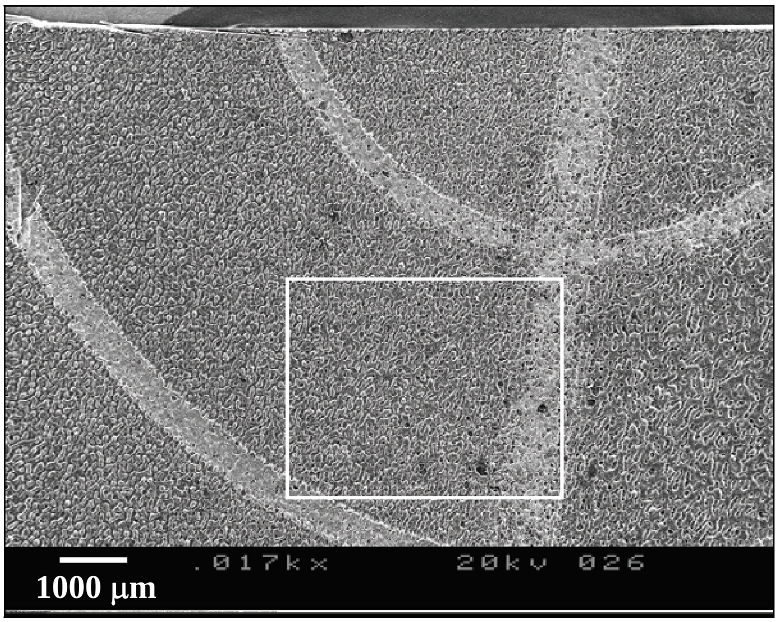

Figure 21. SEM view at magnification 17 of center location (plasma pulse length of 1 ms) showing laser printer lines (white strips) and white box showing approximate location of next higher magnification view.

Figures 23 through 25 show that many particles were deposited in and around the channels and craters. Figures 24 and 25 show particles of two distinctly different morphologies. One particle morphology was spherical and the other was randomly shaped, often with sharp, jagged edges. The randomly shaped particles ranged in size from tens of microns to submicrons. The spherical particles were found to be only in the range of a few microns to approximately 10 microns in size. Figure 25 shows an especially good example of a spherical particle in proximity to a much larger jagged particle.

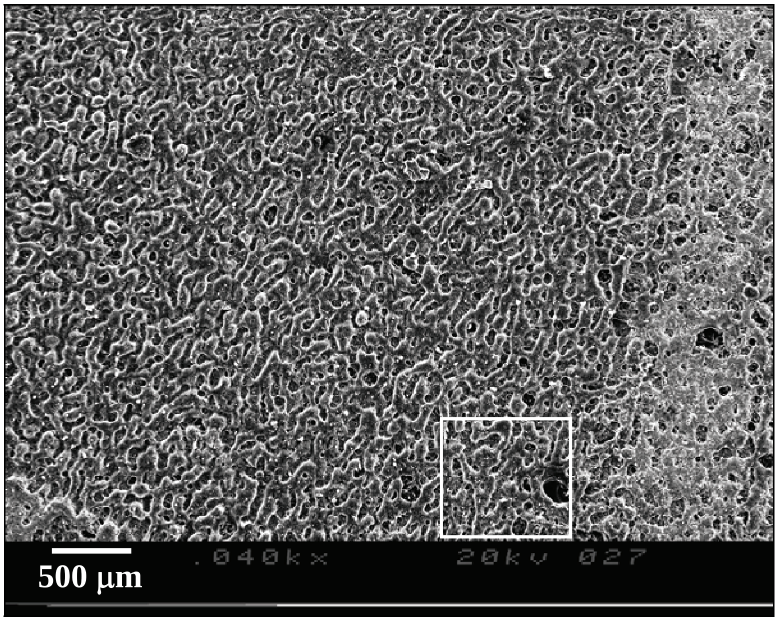

Figure 22. SEM view at magnification 40 of center location (plasma pulse length of 1 ms) with white box showing approximate location of next higher magnification view

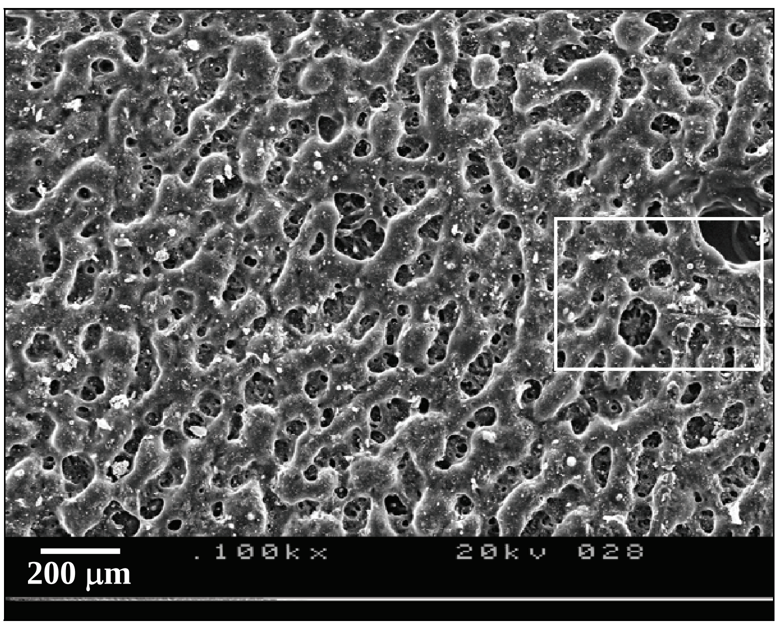

Figure 23. SEM view at magnification 100 of center location (plasma pulse length of 1 ms) with white box showing approximate location of next higher magnification view.

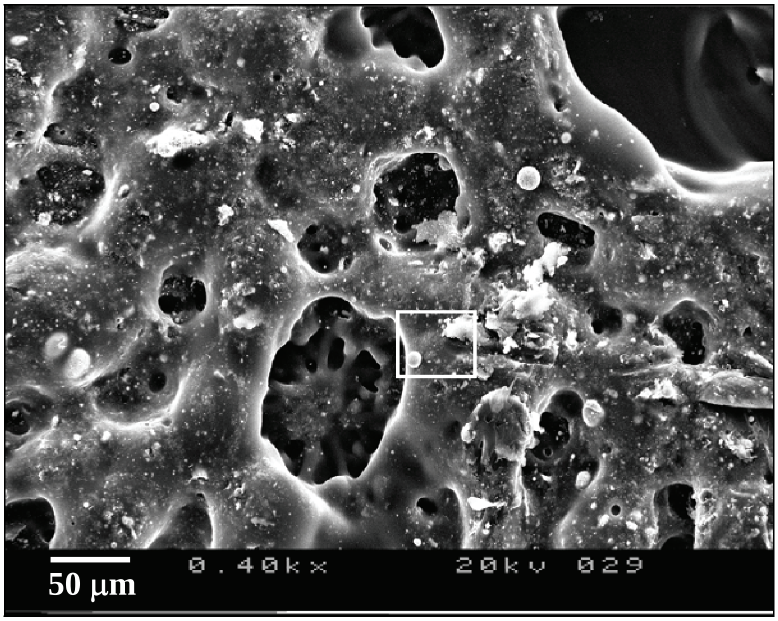

Figure 24. SEM view at magnification 400 of center location (plasma pulse length of 1 ms) with white box showing approximate location of next higher magnification view

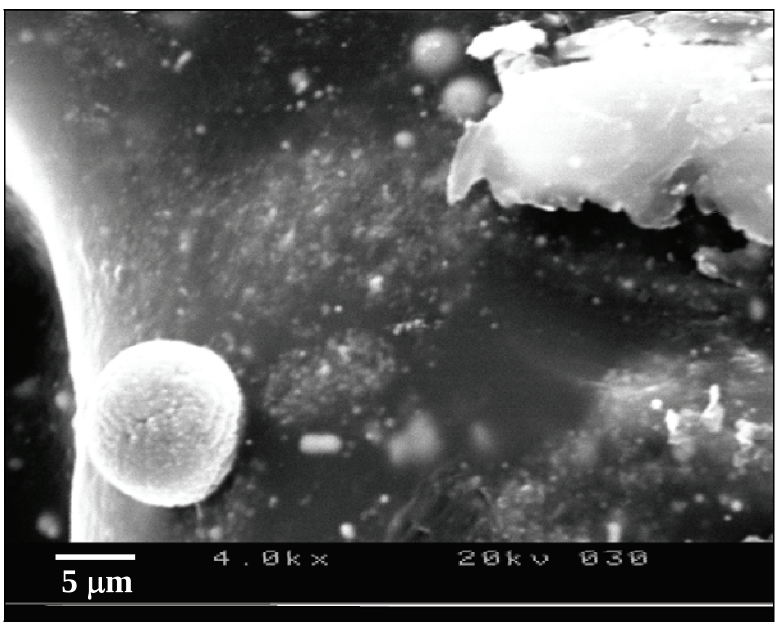

Figure 25. SEM view at magnification 4,000 of center location (plasma pulse length of 1 ms).

When the plasma jet pulse was shortened to 0.3 ms, it was expected from figures 5 through 8 (the shorter pulse was much brighter and thus possibly hotter than the longer pulse) that more extensive thermal damage would be found close to the impingement center and less at larger radii than was found with a pulse length of 1 ms. Indeed, thermal damage was not noticed to any degree at the 6-cm radius location for the shorter pulse (figures 28 through 31) when it was examined.

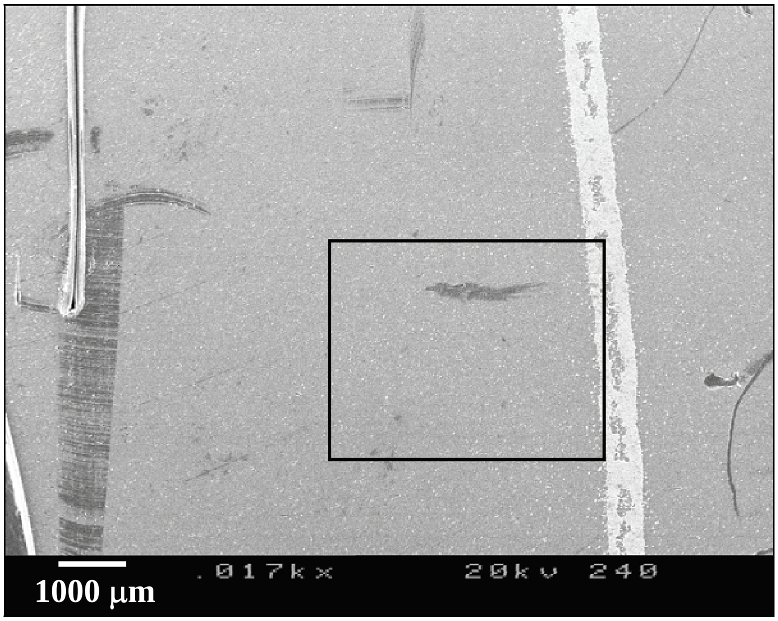

Figure 26. SEM view at magnification 17 of a 6-cm location (plasma pulse length of 0.3 ms) showing laser printer line (white strip) and black box showing approximate location of next higher magnification view

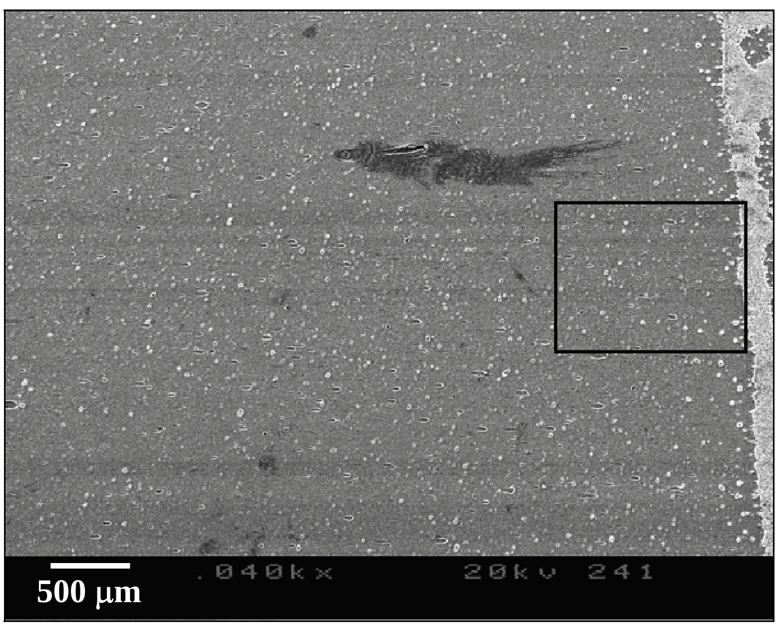

Figure 27. SEM view at magnification 400 of a 6-cm location (plasma pulse length of 0.3 ms) showing laser printer line (white strip at right) and black box showing approximate location of next higher magnification view.

However, more gouge tracks were found than for the case of the longer pulse (compare figures 28 and 18). As in figure 18, all gouge tracks were directed outwardly from the impingement center. Assuming a C_∞ symmetry about the impingement axis for both the long and short pulses, a comparison of figures 28 and 18 would indicate that particles that had sufficient mass and internal energy to create this damage were roughly twice as prevalent in the shorter pulse at this radius.

It is probable that the particles that created the gouge tracks were metal. Metal particles should have the greatest possible mass of particles generated in the plasma (the atomic weight of the majority metal would be that of Fe at 56 daltons versus 12 for C). Since the gouge tracks were all smooth walled without oscillations that would be present if the particle were irregularly shaped, it was inferred that spherical particles created the tracks instead of the jagged particles. Molten metal particles, such as those formed in shot towers, tend to form spherical particles, whereas carbon in hot dynamic environments tends to form sooty particles such as lampblack.

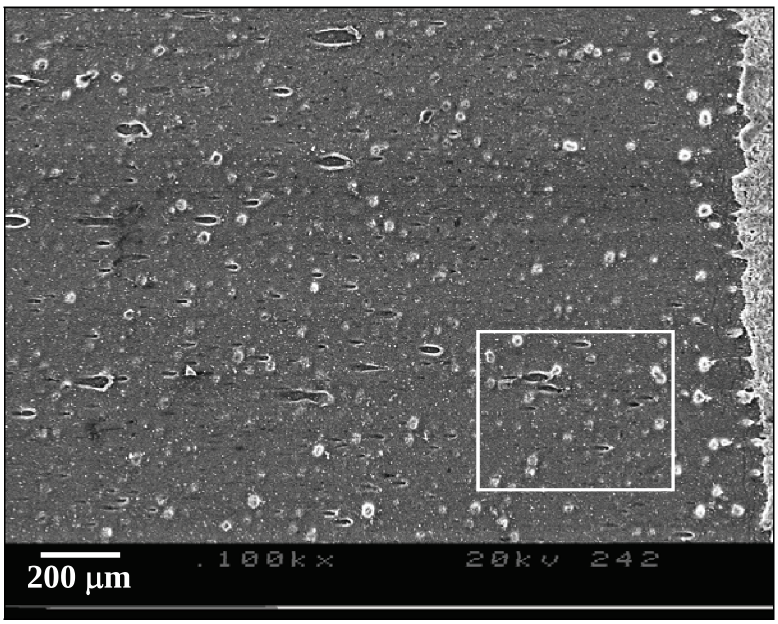

Figure 28. SEM view at magnification 100 of a 6-cm location (plasma pulse length of 0.3 ms) showing laser printer line (white strip at right) and white box showing approximate location of next higher magnification view.

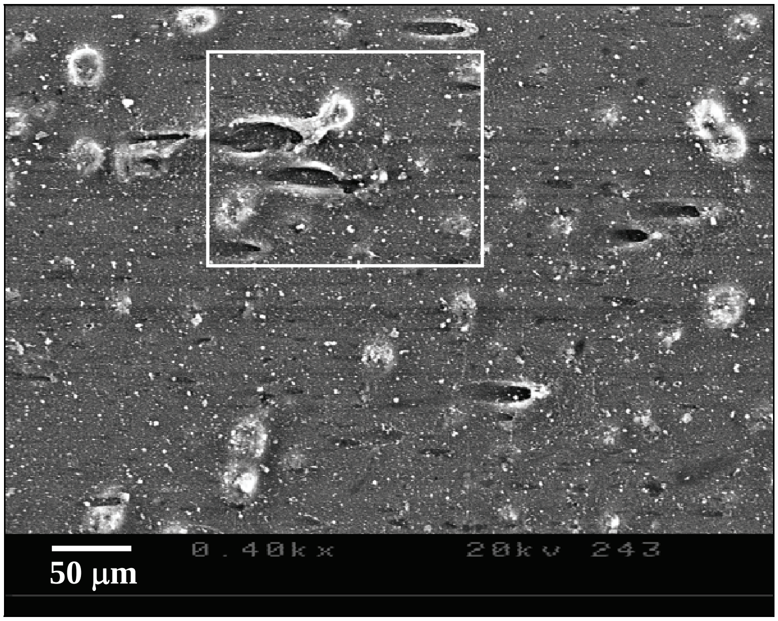

Figure 29. SEM view at magnification 400 of a 6-cm location (plasma pulse length of 0.3 ms) with white box showing approximate location of next higher magnification view.

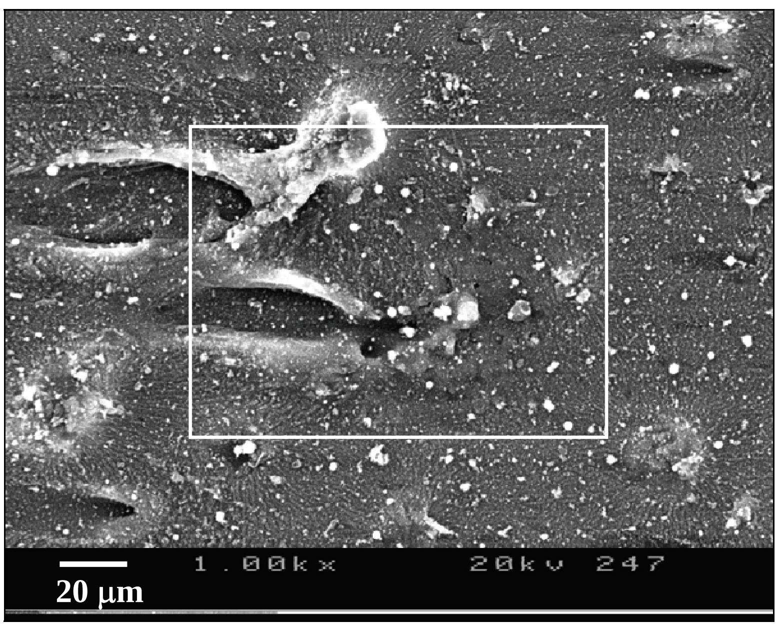

Figure 30. SEM view at magnification 1,000 of a 6-cm location (plasma pulse length of 0.3 ms) with white box showing approximate location of next higher magnification view.

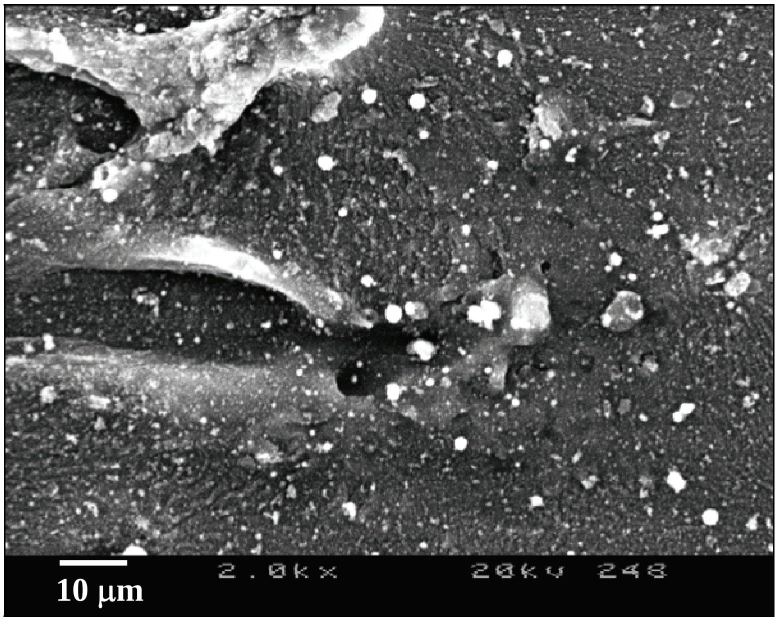

Figure 31. SEM view at magnification 2,000 of a 6-cm location (plasma pulse length of 0.3 ms).

The impingement center of the shorter pulse was more heavily damaged than for the longer pulse (compare figures 32 and 21). The toner ink from the laser printer that marked the radii circles was mostly removed in figure 32. There are more large craters in figure 32 that appear to penetrate more deeply than in figure 21. Fewer of the smallest particles appear to be trapped in the channels in figure 34 (short pulse) than in figure 23 (long pulse). If the flow velocity were greater with the shorter pulse, lighter particles might have had a greater chance to be swept away and the channels "scoured" cleaner than with lower flow velocities present in the long pulse. Indeed, figure 24 (long pulse) shows greater diversity in particle shapes and sizes than in figure 34 (short pulse) as well as a greater number of particles on the surface. Figures 35 and 36 show that only large particles remain on the surface. Other, extremely fine particles appear to form a "crust" within the upper layer of the surface material. Whether this crust indicates partial decomposition of the surface material because of the extreme thermal environment or an efficient mechanism of particle capture in a molten surface is indeterminate at this point.

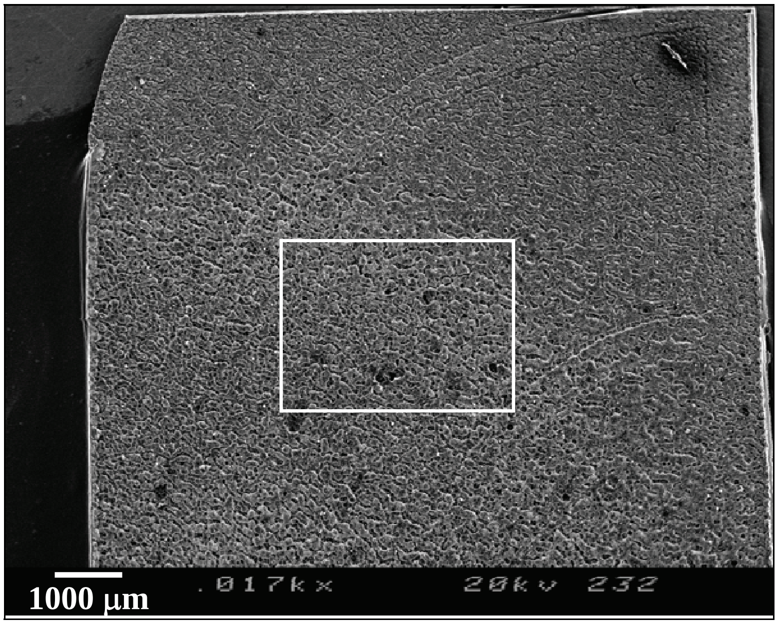

Figure 32. SEM view at magnification 17 of center location (plasma pulse length of 0.3 ms) showing laser printer lines (semi-circles) and white box showing approximate location of next higher magnification view.

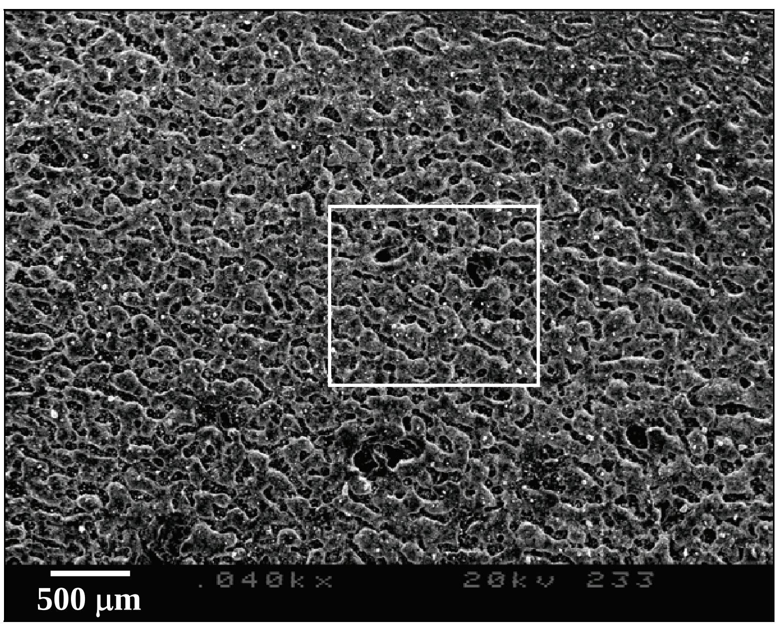

Figure 33. SEM view at magnification 400 of center location (plasma pulse length of 0.3 ms) with white box showing approximate location of next higher magnification view.

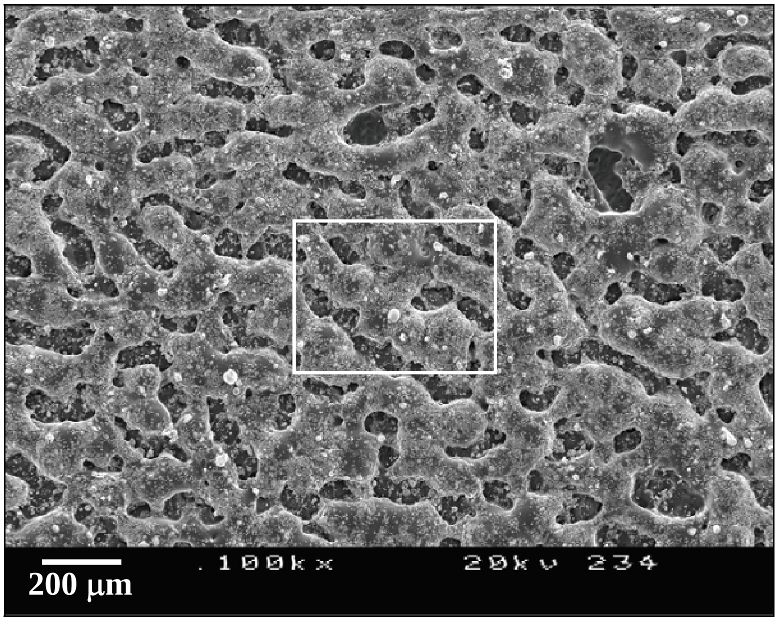

Figure 34. SEM view at magnification 100 of center location (plasma pulse length of 0.3 ms) with white box showing approximate location of next higher magnification view.

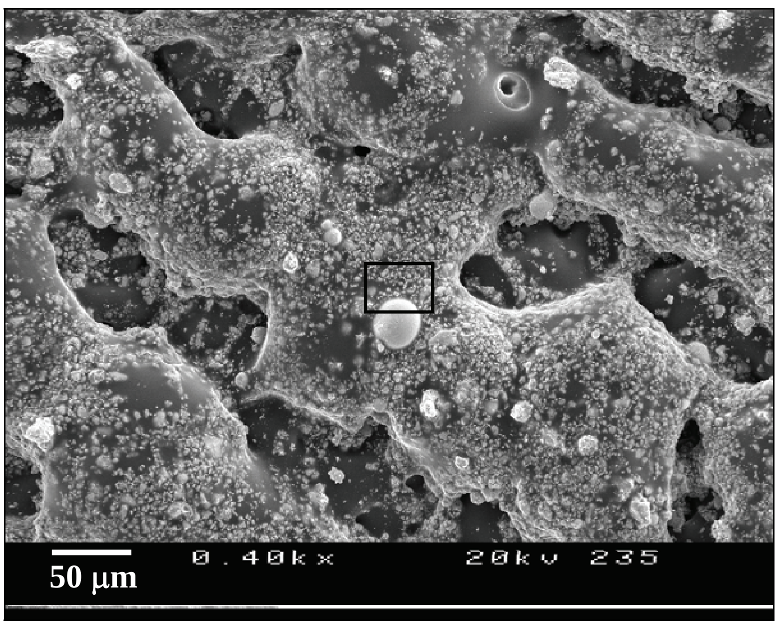

Figure 35. SEM view at magnification 400 of center location (plasma pulse length of 0.3 ms) with black box showing approximate location of next higher magnification view.

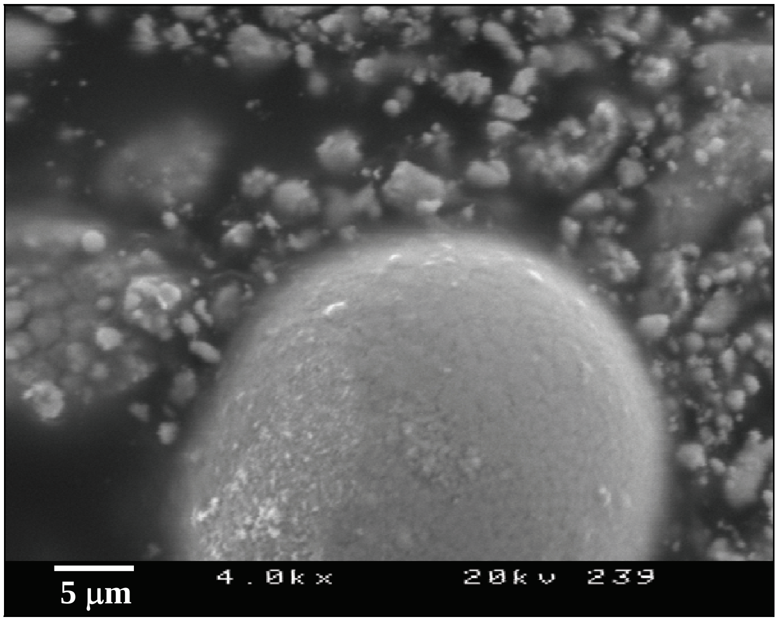

Figure 36. SEM view at magnification 4,000 of center location (plasma pulse length of 0.3 ms).

With the discussed mechanisms of particle capture, comparisons of the effectiveness of particle deposition from the plasma jet at the different incidence angles and pulse lengths can be made. Since the plasma generator operates in a severely choked mode, it was assumed that the behavior of the plasma generator depended on plasma energy and possibly pulse length but not on the angle at which the jet impinged the witness plate. Therefore, the particle generation (especially that of metal particles) should be essentially constant over the range of angles investigated.

After the plasma jet had impinged the witness plate, the witness plate was scanned (figures 4 and 9 through 13) in bitmap mode. The contribution of the spatial reference circles was removed and the spectral density was obtained with the virgin witness material as spectral reference.

After the spectral density was obtained for each pulse length (0.3 and 1 ms) and for each energy (0.7 and 1.3 kJ) at each of the three incident angles (90, 60, and 45 degrees), figures 37 through 40 were prepared in order to compare the effectiveness of particle deposition.

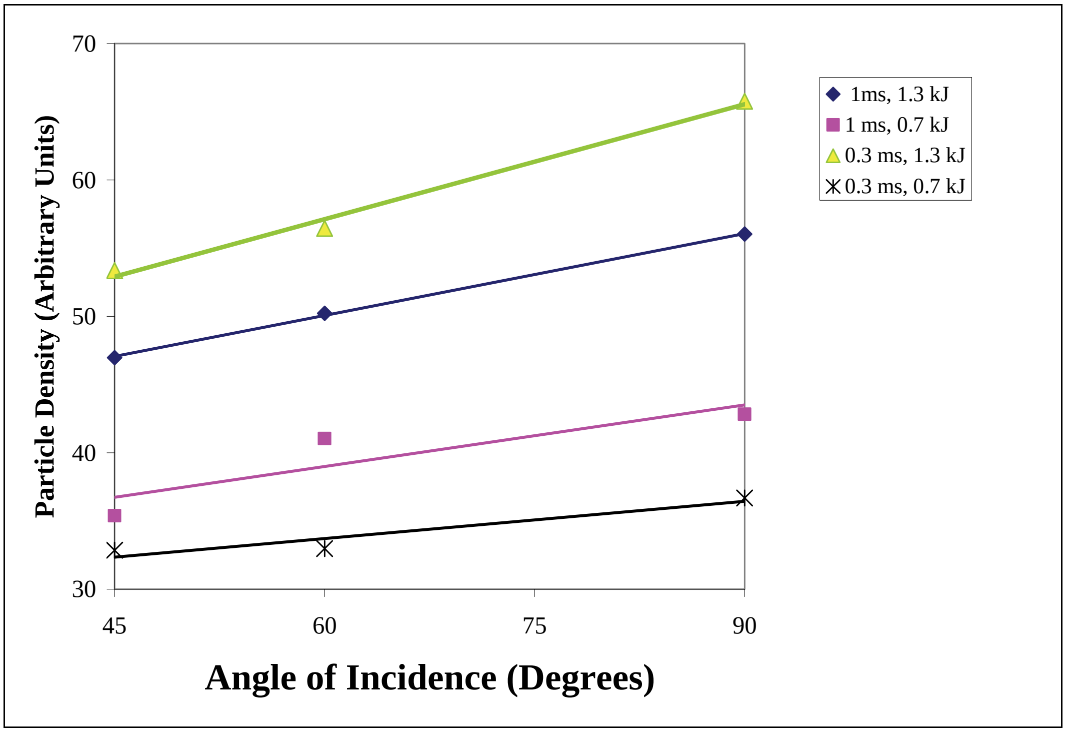

Figure 37. Comparison of particle deposition as a function of angle of incidence for varying energy and pulse duration.

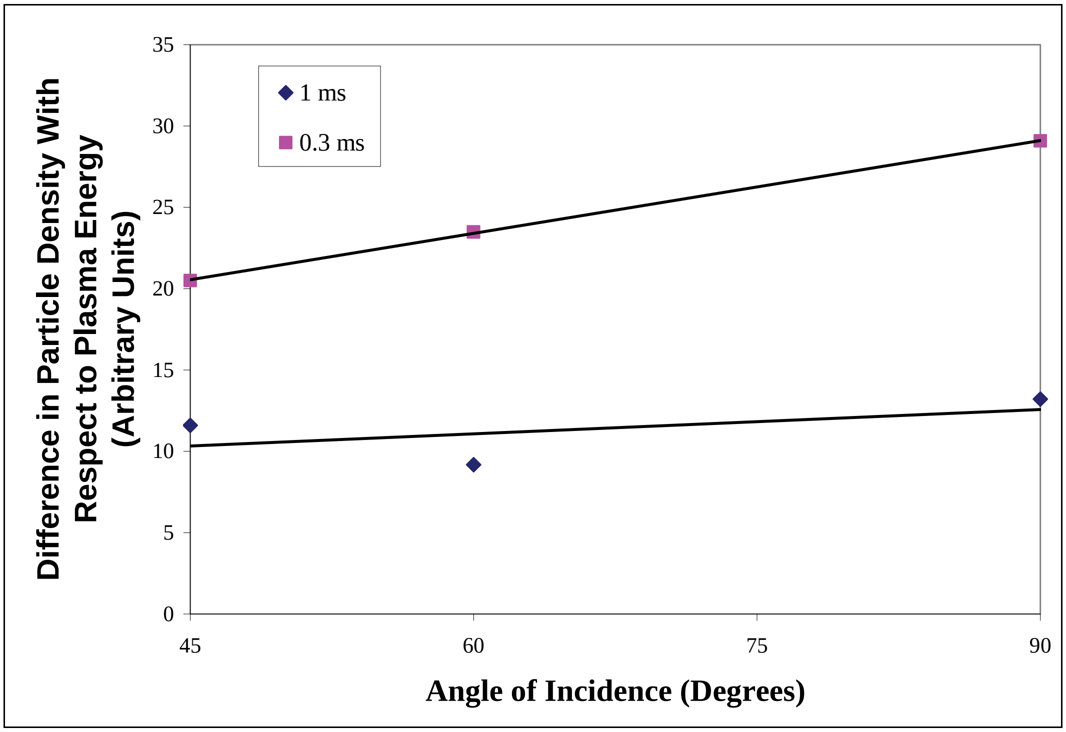

Figure 38. Comparison of difference of particle deposition between 0.7 and 1.3 kJ as a function of angle of incidence at constant pulse length.

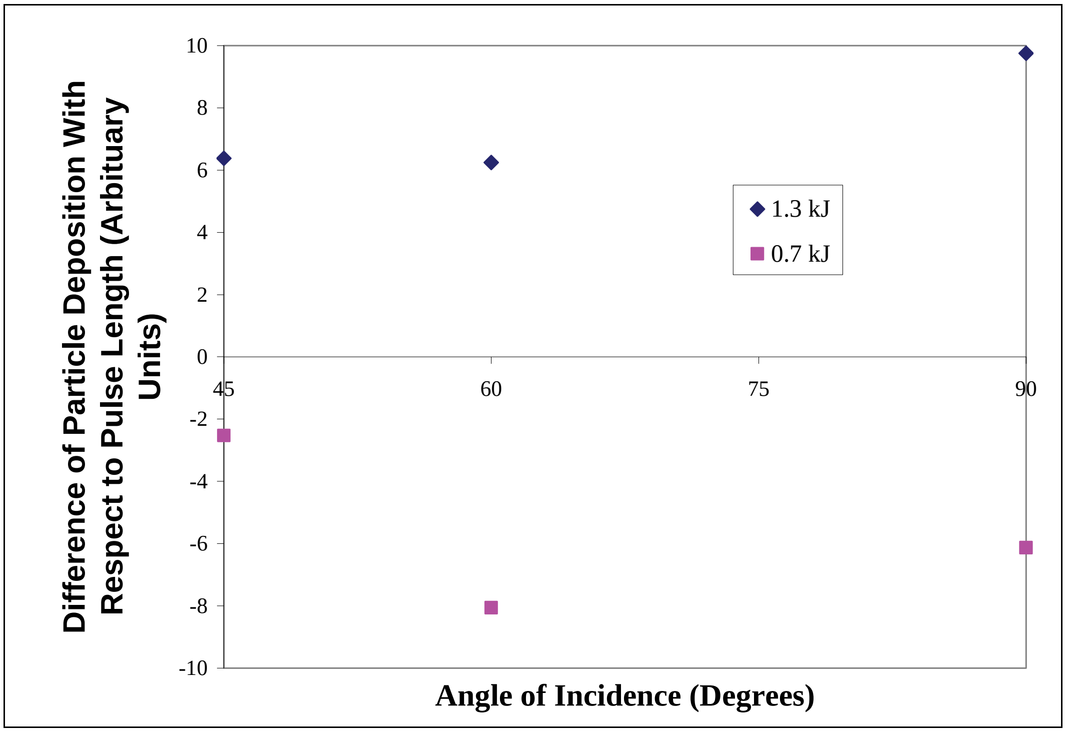

Figure 39. Comparison of difference of particle deposition between 0.3 and 1 ms as a function of angle of incidence at constant energy.

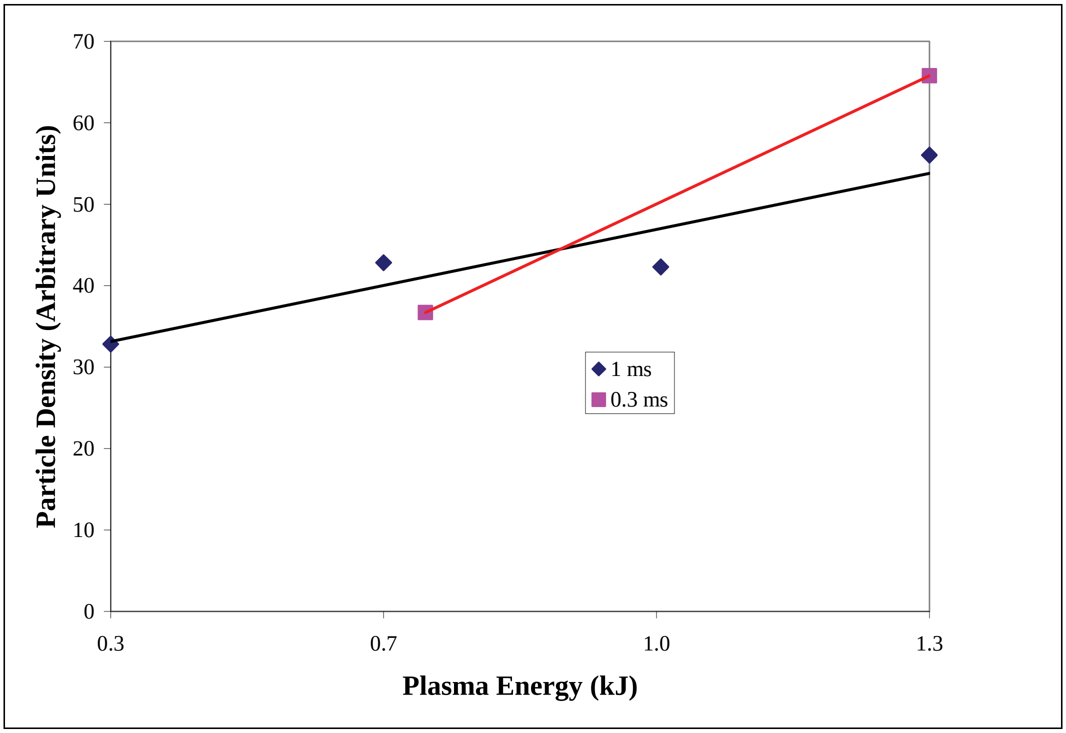

Figure 40. Comparison of particle deposition as a function of plasma energy at an angle of incidence of 90 degrees and at constant pulse length.

It appeared that for the most part, that the number of particles deposited on the impingement surface increased with both angle of incidence and energy. Figure 40 shows that at a given angle of incidence (90 degrees) and pulse length, the amount of particles deposited increased with energy (0.3 to 1.3 kJ). In this energy range, the Powell model (*9*) showed that as the energy increased, more capillary wall material was ablated and more carbon was formed in the gas phase. As the plasma cooled upon exiting the capillary, the carbon began to condense into clusters that formed larger and larger particles until an equilibrium distribution of sizes was formed. The total mass of metal particles was probably also determined by both plasma energy and pulse length since the primary mechanisms for metal removal should be melting/sublimation and erosion. Therefore, it is possible that more metal particles may be formed as the plasma energy increases and/or the pulse length increases.

Even though the data set for the 0.3-ms pulse length in figure 40 was not completed at the time of publication for this report, there appears to be a cross-over point in energy when the short pulse length would deposit as many particles (metal/carbon ratio was not determinable in this study) as the long pulse. This point could be used if hardware and pulse power supply configuration requirements were restrictive. However, it must also be remembered that the amount of surface deformation also depends upon plasma duration (refer to figures 16 through 36) and may, by extension, be assumed to also depend upon plasma energy. This cross-over point in pulse length/plasma energy could be a point at which optimization for a particular ignition system could begin.

It is interesting to note that in figures 37 and 38, the angular dependence of particle deposition appeared to be linear instead of sinusoidal. This effect could be because the impinging jet tended to follow the contour of the impinging surface instead of directly reflecting off the surface. However, when the difference in the amount of particle deposition between the two pulse lengths was compared at each angle of incidence and at constant plasma energy (figure 39), the relationship was possibly nonlinear.

All the results in this study were done at ambient temperatures (at or near 25 °C). Propellants are used over a much broader temperature range. Full studies should also include the measurements described in this study at more extreme temperatures such as -30 °C or 70 °C.

4. Summary

As a limiting geometry, the flat plate was chosen as an impingement surface upon which to observe the particle deposition from an effusive plasma jet. Witness material was chosen with the characteristics of melting point close to the melting/decomposition temperature of typical propellants, relatively soft surface comparable to that of double-base propellants, and high transparency so that particle deposition and surface damage could readily be observed. The material also required a low heat capacity and thermal transmission comparable to those of typical propellants.

High-speed video showed complex flow and shock structures at the energies and incidence angles studied. Correlations were obtained which demonstrated that the plasma energy and the length of the plasma pulse can interact in a convoluted manner that may require more work in order to optimize a particular ignition system. If particle interaction with a particular propellant is important to its successful ignition, this optimization would be required to be performed.

Surface damage to the witness plate material indicated that metal particle distributions in the plasma jet may highly influence propellant surface deformation and energy deposition during the early stages of propellant ignition. Surface damage to the propellant by the particles and the hot gases may provide a mechanism by which electro-thermal igniters have shown compensation for the conventional temperature dependence of propellant burn rates. This compensation can provide a nearly uniform ballistic performance in some guns across a wide range of operating temperatures.

Further examination of the surface deformations created by impingement of plasma jets upon a propellant (simulated or energetic) should remain a priority until the temperature compensation mechanism(s) can be determined and understood. Revisiting this study at temperature extremes to demonstrate if increased deformations occur at cold temperatures and decreased deformations at hot temperatures would probably be beneficial. After the mechanism(s) is(are) understood, engineering solutions can be used to optimize propellant-fueled weapon systems and increase ballistic performance.

5. References

1. Chang, L.-M.; Howard, S. L. *Influence of Pulse Length on Electro-Thermal Plasma Jet Impingement Flow*; ARL-TR-4348; U.S. Army Research Laboratory: Aberdeen Proving Ground, MD, December 2007.

2. Beyer, R.; Pesce-Rodriguez, R. A. The Response of Propellants to Plasma Radiation. *IEEE Journal of Magnetics*, **2005,** *41* (1), 344-349.

3. Schroeder, M. E.; Beyer, R. A.; Pesce-Rodriguez, R. A. Scanning Electron Microscope Examination of JA2 Propellant Samples Exposed to Plasma Radiation. *IEEE Journal of Magnetics*, **2005,** *41* (1), 350-354.

4. Taylor, M. J. Consideration of the Energy Transfer Mechanisms Involved in SPETC Ignition Systems. *IEEE Trans. Magn.*, **2003,** *39* (1), 262-268.

5. Howard, S. L.; Chang, L.-M. *Flow Interaction of an Electro-Thermal Plasma with Simulated Solid Propellant*; DEA-A-65-GE-1060; U.S. Army Research Laboratory: Aberdeen Proving Ground, MD, October, 2004.

6. May, I. W.; Horst, A. W. *Charge Design Considerations and Effects on Pressure Waves in Guns*; BRL-TR-0227; U. S. Army Ballistics Research Laboratory: Aberdeen Proving Ground, MD, December 1978.

7. Kooker, D. E.; Howard, S. L.; Chang, L.-M. *Flamespreading in Granular Solid Propellant: Initial Results*; ARL-TR-446; U.S. Army Research Laboratory: Aberdeen Proving Ground, MD, June 1994.

8. Weiser V.; Kelzenberg, S.; Eisenreich, N. Influence of the Metal Particle Size on the Ignition of Energetic Materials. *Propellants, Explosives, Pyrotechnics*, **2001,** *26* (6), 284-289.

9. Powell, J. D., and A. Zielinski. *Theory and Experiment for an Ablating-Capillary Discharge and Application to Electrothermal-Chemical Guns*; BRL-TR-3355; U.S. Army Ballistics Research Laboratory: Aberdeen Proving Ground, MD, June 1992.

NO. OF COPIES	ORGANIZATION
1 (PDF ONLY)	DEFENSE TECHNICAL INFORMATION CTR DTIC OCA 8725 JOHN J KINGMAN RD STE 0944 FORT BELVOIR VA 22060-6218
1	US ARMY RSRCH DEV & ENGRG CMD SYSTEMS OF SYSTEMS INTEGRATION AMSRD SS T 6000 6TH ST STE 100 FORT BELVOIR VA 22060-5608
1	DIRECTOR US ARMY RESEARCH LAB IMNE ALC IMS 2800 POWDER MILL RD ADELPHI MD 20783-1197
1	DIRECTOR US ARMY RESEARCH LAB AMSRD ARL CI OK TL 2800 POWDER MILL RD ADELPHI MD 20783-1197
2	DIRECTOR US ARMY RESEARCH LAB AMSRD ARL CI OK T 2800 POWDER MILL RD ADELPHI MD 20783-1197
1	US MILITARY ACADEMY DEPT CVL AND MECHL ENGRG ATTN COL J SAMPLES MAHAN HALL OFC 322 WEST POINT NY 10996
2	CDR ARO TECH LIBRARY ATTN D MANN PO BOX 12211 RSCH TRIANGLE PARK NC 27709-2211
2	COMMANDER RDECOM ARDEC ATTN AMSRD AR WEE S MOY A ENG BLDG 382 PICATINNY ARSENAL NJ 07806-5000
1	DIRECTOR US ARMY RESEARCH LAB ATTN AMSRD ARL RO P R SHAW TECH LIB PO BOX 12211 RSCH TRIANGLE PARK NC 27709-2211

NO. OF COPIES	ORGANIZATION
1	COMMANDER NAVAL RSRCH LAB TECH LIB WASHINGTON DC 20375-5000
1	OFFICE OF NAVAL RSRCH J GOLDWASSER 875 N RANDOLPH ST RM 653 ARLINGTON VA 22203-1768
1	PA STATE UNIV DEPT OF MECH ENGRG ATTN S T THYNELL 309 REBER BLDG UNIVERSITY PARK PA 16802
1	COMMANDER US ARMY ARDEC ATTN AMSRD AAR AED I J HIRLINGER BLDG 65 PICATINNY ARSENAL NJ 07806-5000
2	COMMANDER RDECOM ARDEC ATTN AMSRD AR WEE W P HUI L CHANG BLDG 328 PICATINNY ARSENAL NJ 07806-5000
2	COMMANDER DRPM AAA FIRE POWER WORTH AVE TECH CENTER ATTN MAJ K MULLINS LTC P W CUSHING 14041 WORTH AVE WOODBRIDGE VA 22192
1	COMMANDER NAVAL SURFACE WARFARE CTR TECH LIB BLDG 299 INDIAN HEAD MD 20640-5035
1	COMMANDER NAVAL SURFACE WARFARE CTR TECH LIB DAHLGREN VA 22448-5000
1	COMMANDER NAVAL SURFACE WARFARE CTR TECH LIB 101 STRAUSS AVE INDIAN HEAD MD 20640-5000

NO. OF COPIES	ORGANIZATION
1	COMMANDER RADFORD ARMY AMMUNITION PLANT ATTN SMCAR QA HI LIB RADFORD VA 24141-0298
1	COMMANDER NAVAL AIR WARFARE CTR INFORMATION SCIENCE DIV CHINA LAKE CA 93555-6001
1	SRI INTERNATIONAL TECH LIB PROPULSION SCIENCES DIV 333 RAVENWOOD AVE MENLO PARK CA 94025-3493

ABERDEEN PROVING GROUND

1	DIRECTOR US ARMY RSCH LABORATORY ATTN AMSRD ARL CI OK (TECH LIB) BLDG 4600
20	DIR USARL AMSRD ARL WM M J BEATTY B RINGERS J SMITH AMSRD ARL WM MC R ADLER AMSRD ARL WM BA F BRANDON AMSRD ARL WM BC B GUIDOS AMSRD ARL WM BD R BEYER J COLBURN P CONROY A BRANT S HOWARD (3 CYS) M NUSCA B FORCH A WILLIAMS P KASTE R PESCE-RODRIGUEZ A HORST L M CHANG